Published in final edited form as:

Clin Cancer Res. 2023 July 05; 29(13): 2540–2550. doi:10.1158/1078-0432.CCR-22-3413.

Corresponding Authors: Michael L. Cheng, Helen Diller Family Comprehensive Cancer Center, University of California, San Francisco, 550 16th Street, San Francisco, CA 94158. michael.cheng@ucsf.edu; and Biagio Ricciuti, Lowe Center for Thoracic Oncology, Dana-Farber Cancer Institute, Harvard Medical School, 450 Brookline Avenue, Boston, MA 02215. biagio_ricciuti@dfci.harvard.edu.

B. Ricciuti and A. Elkrief contributed equally to this article.

Current address for Michael L. Cheng: Helen Diller Family Comprehensive Cancer Center, University of California, San Francisco, California.

Authors' Contributions

B. Ricciuti: Conceptualization, data curation, software, formal analysis, supervision, funding acquisition, validation, visualization, methodology, writing–original draft, writing–review and editing. **A. Elkrief:** Conceptualization, data curation, supervision, methodology, writing–original draft, writing–review and editing. **J. Alessi:** Conceptualization, data curation, software, formal analysis, methodology, writing–original draft, writing–review and editing. **X. Wang:** Conceptualization, data curation, software, formal analysis, methodology, writing–review and editing. **Y. Li:** Software, formal analysis, methodology, writing–review and editing. **H. Gupta:** Data curation, software, formal analysis, methodology, writing–review and editing. **D.M. Muldoon:** Resources, data curation, formal analysis. **A.A. Bertram:** Data curation, writing–review and editing. **F. Pecci:** Data curation, methodology, writing–original draft, writing–review and editing. **G. Lamberti:** Data curation, formal analysis, supervision, methodology, writing–original draft, writing–review and editing. **A. Di Federico:** Data curation, supervision, writing–original draft, writing–review and editing. **A. Barrichello:** Data curation, writing–original draft, writing–review and editing. **V.R. Vaz:** Resources, data curation, writing–original draft, writing–review and editing. **M. Gandhi:** Data curation, writing–original draft, writing–review and editing. **E. Lee:** Resources, data curation. **G.I. Shapiro:** Conceptualization, data curation, funding acquisition, writing–original draft, project administration, writing–review and editing. **H. Park:** Data curation, writing–original draft, writing–review and editing. **M. Nishino:** Resources, data curation, visualization, methodology, writing–original draft, writing–review and editing. **J. Lindsay:** Resources, data curation, formal analysis, methodology, writing–original draft, writing–review and editing. **K.D. Felt:** Resources, data curation, formal analysis, methodology, writing–original draft, writing–review and editing. **B. Sharma:** Resources, data curation, formal analysis, methodology, writing–original draft, writing–review and editing. **A.D. Cherniack:** Resources, data curation, software, formal analysis, methodology, writing–original draft, writing–review and editing. **S. Rodig:** Resources, data curation, software, formal analysis, methodology, writing–original draft, writing–review and editing. **D.R. Gomez:** Resources, data curation. **N. Shaverdian:** Resources, data curation. **M. Rakaee:** Resources, data curation, software, formal analysis. **C. Bandlamudi:** Resources, data curation, methodology. **M. Ladanyi:** Resources, data curation, methodology. **P.A. Janne:** Resources, supervision, writing–original draft, writing–review and editing. **A.J. Schoenfeld:** Conceptualization, supervision, writing–original draft, writing–review and editing. **L.M. Sholl:** Resources, data curation, formal analysis, writing–original draft, writing–review and editing. **M.M. Awad:** Conceptualization, supervision, methodology, writing–original draft, writing–review and editing. **M.L. Cheng:** Conceptualization, resources, data curation, supervision, funding acquisition, writing–original draft, project administration, writing–review and editing.

Authors' Disclosures

B. Ricciuti reports other support from Regeneron outside the submitted work. A. Elkrief reports grants from Canadian Institutes of Health Research, Royal College of Physicians and Surgeons of Canada, and Cedar's Cancer Foundation during the conduct of the study and personal fees from Merck outside the submitted work. Y. Li reports other support from g.Root Biomedical Services outside the submitted work. G.I. Shapiro reports grants and personal fees from Merck KGaA/EMD-Serono; grants from Tango, Bristol-Myers Squibb, Pfizer, and Eli Lilly; and personal fees from Bicycle Therapeutics, Cybrexa Therapeutics, Boehringer Ingelheim, Bayer, ImmunoMet, Concarlo Holdings, Syros, Zentalis, CytomX Therapeutics, Blueprint Medicines, Kymera Therapeutics, Janssen, Xinthera, and Artios outside the submitted work; in addition, G.I. Shapiro has a patent for Dosage regimen for sapacitabine and seliciclib issued to Cyclacel Pharmaceuticals and a patent for Compositions and methods for predicting response and resistance to CDK4/6 inhibition issued to Liam Cornell and Geoffrey Shapiro. M. Nishino reports grants from AstraZeneca, Canon Medical Systems, and Daiichi Sankyo and personal fees from AstraZeneca outside the submitted work. A.D. Cherniack reports other support from Bayer outside the submitted work. S. Rodig reports grants from KITE/Gilead and Bristol-Myers Squibb outside the submitted work. D.R. Gomez reports grants from Merck, AstraZeneca, Varian, and BMS and personal fees from Med Learning Group, Varian, GRAIL, Olympus, Johnson and Johnson, Medtronic, and AstraZeneca outside the submitted work. N. Shaverdian reports other support from Novartis outside the submitted work. P.A. Janne reports grants and personal fees from AstraZeneca, Boehringer Ingelheim, Eli Lilly, Daiichi Sankyo, Takeda Oncology; personal fees from Pfizer, Roche/Genentech, Chugai, SFJ Pharmaceuticals, Voronoi, Biocartis, Novartis, Sanofi Oncology, Mirati Therapeutics, Transcenta, Silicon Therapeutics, Syntax, Nuvalent, Bayer, Eisai, Allorion Therapeutics, Accutar Biotech, AbbVie, Monte Rosa, Scorpion Therapeutics, Merus, Frontier Medicines, Hongyun Biotechnology, Duality; and grants from PUMA and Revolution Medicines outside the submitted work; in addition, P.A. Janne has a patent for EGFR mutations issued and licensed to LabCorp. A.J. Schoenfeld reports personal fees from J&J, KSQ therapeutics, Perceptive Advisors, Oppenheimer and Co., Umoja Biopharma, Legend Biotech, Prelude Therapeutics, Lyell Immunopharma, Heat Biologics; grants and personal fees from BMS, Merck, Iovance Biotherapeutics, Amgen; and grants from Achilles Therapeutics, PACT pharma, and Harpoon Therapeutics outside the submitted work. L.M. Sholl reports grants and personal fees from Genentech; grants from Bristol-Myers Squibb; and personal fees from Astra Zeneca, GV20 Therapeutics and Lilly outside the submitted work. M.M. Awad reports personal fees from Merck, ArcherDx, Mirati, Gritstone, AstraZeneca, Novartis, EMD Serono, and Nektar; grants and personal fees from Genentech, Bristol-Myers Squibb, and Amgen; and grants from Lilly; during the conduct of the study. M.L. Cheng reports personal fees from AstraZeneca, Boehringer Ingelheim, Pfizer, Mirati Therapeutics, Cepheid, Janssen, and Potomac Center for Medical Education and grants from Palleon Pharmaceuticals outside the submitted work. No disclosures were reported by the other authors.

Clinicopathologic, Genomic, and Immunophenotypic Landscape of *ATM* Mutations in Non–Small Cell Lung Cancer

Biagio Ricciuti[1], **Arielle Elkrief**[2], **Joao Alessi**[1], **Xinan Wang**[3], **Yvonne Li**[4], **Hersh Gupta**[4], **Daniel M. Muldoon**[2], **Arrien A. Bertram**[1], **Federica Pecci**[1], **Giuseppe Lamberti**[1], **Alessandro Di Federico**[1], **Adriana Barrichello**[1], **Victor R. Vaz**[1], **Malini Gandhi**[1], **Elinton Lee**[1], **Geoffrey I. Shapiro**[5], **Hyesun Park**[6], **Mizuki Nishino**[6], **James Lindsay**[7], **Kristen D. Felt**[7], **Bijaya Sharma**[7], **Andrew D. Cherniack**[4], **Scott Rodig**[8], **Daniel R. Gomez**[9], **Narek Shaverdian**[9], **Mehrdad Rakaee**[10], **Chaitanya Bandlamudi**[2], **Marc Ladanyi**[2], **Pasi A. Janne**[1], **Adam J. Schoenfeld**[2], **Lynette M. Sholl**[8], **Mark M. Awad**[1], **Michael L. Cheng**[1]

[1]Lowe Center for Thoracic Oncology, Dana-Farber Cancer Institute, Harvard Medical School, Boston, Massachusetts.

[2]Thoracic Oncology Service, Department of Medicine, Memorial Sloan Kettering Cancer Center, New York, New York.

[3]Harvard T.H. Chan School of Public Health, Harvard University, Boston, Massachusetts.

[4]Department of Analytics and Informatics, Dana-Farber Cancer Institute, Boston, Massachusetts; Cancer Program, Broad Institute of Harvard and Massachusetts Institute of Technology (MIT), Cambridge, Massachusetts.

[5]Center for DNA Damage and Repair (CDDR), Dana-Farber Cancer Institute, Boston, Massachusetts.

[6]Department of Radiology, Brigham and Women’s Hospital, Boston, Massachusetts.

[7]ImmunoProfile, Brigham & Women’s Hospital and Dana-Farber Cancer Institute, Boston, Massachusetts.

[8]Department of Pathology, Brigham and Women’s Hospital, Boston, Massachusetts.

[9]Department of Radiation Oncology, Memorial Sloan Kettering Cancer Center, New York, New York.

[10]Department of Medicine, Brigham and Women’s Hospital, Harvard Medical School, Boston, Massachusetts.

Abstract

Purpose: *ATM* is the most commonly mutated DNA damage and repair gene in non–small cell lung cancer (NSCLC); however, limited characterization has been pursued.

Experimental Design: Clinicopathologic, genomic, and treatment data were collected for 5,172 patients with NSCLC tumors which underwent genomic profiling. ATM IHC was performed on

The publication costs of this article were defrayed in part by the payment of publication fees. Therefore, and solely to indicate this fact, this article is hereby marked “advertisement” in accordance with 18 USC section 1734.

Supplementary data for this article are available at Clinical Cancer Research Online (http://clincancerres.aacrjournals.org/).

182 NSCLCs with *ATM* mutations. Multiplexed immunofluorescence was performed on a subset of 535 samples to examine tumor-infiltrating immune cell subsets.

Results: A total of 562 deleterious ATM mutations were identified in 9.7% of NSCLC samples. *ATM*-mutant (ATM^{MUT}) NSCLC was significantly associated with female sex ($P = 0.02$), ever smoking status ($P < 0.001$), non-squamous histology ($P = 0.004$), and higher tumor mutational burden (DFCI, $P < 0.0001$; MSK, $P < 0.0001$) compared with *ATM*–wild-type (ATM^{WT}) cases. Among 3,687 NSCLCs with comprehensive genomic profiling, co-occurring *KRAS*, *STK11*, and *ARID2* oncogenic mutations were significantly enriched among ATM^{MUT} NSCLCs ($Q < 0.05$), while *TP53* and *EGFR* mutations were enriched in ATM^{WT} NSCLCs. Among 182 ATM^{MUT} samples with ATM IHC, tumors with nonsense, insertions/deletions, or splice site mutations were significantly more likely to display ATM loss by IHC (71.4% vs. 28.6%; $P < 0.0001$) compared with tumors with only predicted pathogenic missense mutations. Clinical outcomes to PD-(L)1 monotherapy ($N = 1,522$) and chemo-immunotherapy ($N = 951$) were similar between ATM^{MUT} and ATM^{WT} NSCLCs. Patients with concurrent *ATM/TP53* mutations had significantly improved response rate and progression-free survival with PD-(L)1 monotherapy.

Conclusions: Deleterious *ATM* mutations defined a subset of NSCLC with unique clinicopathologic, genomic, and immunophenotypic features. Our data may serve as resource to guide interpretation of specific *ATM* mutations in NSCLC.

Introduction

Clinical care for patients with non–small cell lung cancer (NSCLC) is increasingly defined by precision oncology; however, current standard treatment strategies in this disease do not include targeted therapy approaches involving DNA damage and repair (DDR) (1). Defective DDR machinery is a hallmark of cancer (2, 3) and aberrations involving the ataxia telangiectasia mutated (ATM) kinase are among the most commonly observed DDR defects across cancer types (2). The *ATM* gene encodes a member of the phosphatidylinositol-3 kinase-like (PIKK) family of serine/threonine kinases which senses and mediates the response to DNA double-strand breaks (4–7).

In NSCLC, *ATM* is mutated in up to ~10% of cases, representing the most commonly mutated DDR gene (7–9). Furthermore, ATM protein expression loss in prior studies has been reported in up to 41% of tumors (10–12), though subsequent studies have proposed the potential for overestimation related to challenges with IHC protocol optimization and the inability to detect low expressors which retain full ATM function (13). ATM deficiency has been shown to be synthetic lethal with ataxia telangiectasia and Rad3-related (ATR) inhibition and a number of ATR inhibitors are in early clinical development (14–20). A phase I study of BAY 1895344 monotherapy in advanced solid tumors demonstrated four partial responses with a median duration of response of 315.5 days, all in patients with tumors demonstrating ATM protein loss and/or deleterious mutations in *ATM* (tumor types included appendix, breast, endometrial, and urothelial duct cancers; ref. 18). A phase I study of M6620 in advanced solid tumors included 1 patient with metastatic colorectal cancer which demonstrated ATM IHC loss (alongside an *ARID1A* mutation) who achieved a complete response to M6620 monotherapy, with progression-free survival (PFS) ongoing for 29+ months (17). A phase I study of berzosertib in combination with

cytotoxic chemotherapy in advanced solid tumors includes a partial response in a lung adenocarcinoma patient (ATM status not reported) who received berzosertib + gemcitabine (20). A single arm expansion cohort of berzosertib + gemcitabine in advanced NSCLC demonstrated a modest objective response rate (ORR) of 10.5%. However, the trial population included only single digit cases harboring *ATM* mutations and planned ATM IHC was not possible due to exhaustion of tissue (19). Separately, emerging data from our group and others suggest that deleterious DDR mutations may predict for improved outcomes to PD-(L)1 immune checkpoint blockade in NSCLC (21, 22); however, *ATM*-specific analyses have not been pursued.

ATM is a notably large gene, and mutations occur throughout the gene with no clear hotspots, with very limited functional characterization of specific variants. Comprehensive analyses integrating genomic as well as IHC and other biomarker data with patient outcomes have not yet been pursued, and it is unknown which *ATM* variants may represent actionable biomarkers in NSCLC. Here, we characterize the clinicopathologic, genomic, and immunophenotypic landscape of *ATM* mutations in a large multi-institutional cohort of patients with NSCLC with the goal of informing future DDR-based targeted therapy strategies as well as precision oncology approaches involving other systemic therapies, including PD-(L)1 immune checkpoint blockade.

Materials and Methods

Study design and patients

Clinicopathologic and genomic data were collected from patients with NSCLC who had provided written informed consent to institutional review board—approved correlative research studies at the Dana-Farber Cancer Institute [DFCI; Dana-Farber/Harvard Cancer Center (DF/HCC) protocols #02–180, #11–104, #13–364, and/or #17–000], and Memorial Sloan Kettering Cancer Center (MSK; protocol #12–245), and whose tumors underwent comprehensive tumor genomic profiling at each of the participating institution. This study was conducted in accordance with the Declaration of Helsinki.

Tumor genomic profiling

NSCLCs at DFCI were sequenced by targeted next-generation sequencing (NGS) using OncoPanel (23), which interrogates for 277 (v1, 4/2013–07/2014), 302 (v2, 07/2014–09/2016), and 447 (v3, 09/2016-ongoing) cancer-associated genes. DNA was isolated from tumor samples with a tumor purity ≥ 20% and analyzed by massively parallel sequencing using a solution-phase Agilent SureSelect hybrid capture kit and an Illumina HiSeq 2500 sequencer (23, 24). Common single nucleotide polymorphisms present in public and internal non-cancer populations were filtered out algorithmically using an internal informatic pipeline, as previously described (23, 24). NSCLC samples at MSK were sequenced using the MSK-IMPACT platform, detecting single-nucleotide variants, copy-number variations, gene fusions, and insertion/deletions (ins/del) from 341 (v1), 410 (v2), and 468 (v3) unique cancer-associated genes (25).

Programmed death-ligand 1 expression and tumor mutational burden assessment

Programmed death-ligand 1 (PD-L1) expression was reported as a percentage of tumor cells with positive membranous staining in a slide containing at least 100 tumor viable cells using validated anti–PD-L1 antibodies: E1L3N (Cell Signaling Technology, Danvers, MA), 22C3 (Dako North America Inc, Carpinteria, CA), 28–8 (Epitomics Inc, Burlingame, CA), according to local institutional practice. Tumor mutational burden (TMB), defined as the number of somatic, coding, base substitution and ins/del mutations per megabase (Mb) of genome examined was calculated from the DFCI OncoPanel NGS.

Determination of *ATM* mutation status

All loss-of-function mutations in the *ATM* gene, including nonsense, ins/del, or splice site were classified as deleterious. Missense mutations were considered deleterious if deemed to be pathogenic using Polymorphism Phenotyping v2 (PolyPhen-2), a tool which determines the impact of amino acid substitutions on the stability and function of human proteins using structural and comparative evolutionary considerations. PolyPhen-2 performs functional annotation of SNPs, maps coding SNPs to gene transcripts, extracts protein sequence annotations and structural attributes, and builds conservation profiles. It then estimates the probability of the missense mutation being damaging based on a combination of all these properties. Missense mutations not deemed to be pathogenic by PolyPhen-2 were considered benign. Cases harboring at least one deleterious *ATM* mutation were defined *ATM*-mutant (ATM^{MUT}), while cases without *ATM* mutations or harboring only *ATM* mutations considered benign were defined *ATM*–wild-type (ATM^{WT}). A putative loss of heterozygosity (LOH) of *ATM* was defined by the concomitant presence of a deleterious *ATM* mutation and *ATM* deletion, suggesting biallelic inactivation. The DFCI OncoPanel and the MSK-IMPACT NGS platforms have full exonic coverage of the *ATM* gene, and also interrogate approximately 100 base pairs into the introns flanking each exon.

Determination of ATM expression by IHC

NSCLC samples harboring *ATM* mutations and sufficient tissue available for additional studies underwent ATM IHC. Four- to 5-μm thick formalin-fixed, paraffin embedded (FFPE) tissue specimens were prepared from a representative clinical tissue block. Slides were baked at 37°C. Heat-induced epitope retrieval was performed in EDTA for 20 minutes (Leica H2, Leica, Buffalo Grove, IL). ATM clone Y170 (Abcam, Waltham, MA) was used at 1:300 dilution with a 60-minute incubation on the Leica Bond III platform. Staining was evaluated by a board-certified anatomic pathologist (L.M. Sholl) and assigned a score of complete loss when all the tumor cells showed absent nuclear staining, heterogeneous loss when at least 10% of tumor cells showed absent nuclear staining, or intact when all tumor cells showed nuclear expression. Samples with ATM expression loss for which internal control staining in benign stromal/inflammatory cells could not be confirmed were excluded from analysis.

Multiplexed immunofluorescence (ImmunoProfile)

Multiplexed immunofluorescence (mIF) was performed on samples from the DFCI by staining 5-micron FFPE whole tissue sections with standard, primary antibodies sequentially

and paired with a unique fluorochrome followed by staining with nuclear counterstain/4',6-diamidino-2-phenylindole (DAPI). All samples were stained for PD-L1 (clone E1L3N), PD-1 [clone EPR4877 (2)], CD8 (clone 4B11), FOXP3 (clone D608R), Cytokeratin (clone AE1/AE3), and DAPI (nuclear counterstain). Each sample had a single slide stained and scanned at 20x resolution by a Vectra Polaris imaging platform. Regions of Interest (ROI) were defined for each image, and only these regions were used for quantitative image analysis. Within each ROI, InForm Image Analysis software (PerkinElmer/Akoya) was run to phenotype and score cells based on biomarker expression. A custom script quantified the number/percentage of cells which are positive for relevant biomarkers in specific tissue regions. Each ROI was divided into one or more of these defined regions: intra-tumoral (IT), which was defined as the region of the slide consisting of tumor beyond the tumor-stroma interface (TSI); TSI, which was defined as the region within 40 μm to either side of the defined border between tumor and stroma; and total (IT + TSI). Cell count was calculated per ROI and averaged (unweighted) across ROIs, reported as count per millimeter squared ± standard error. Statistical significance of differential cell type enrichment between groups was estimated with Wilcox Rank Sum test.

Immune cell subset estimation from The Cancer Genome Atlas

The association between *ATM* mutation status and immune infiltrates were evaluated in The Cancer Genome Atlas (TCGA) Program. Immune cell infiltration levels of each patient with lung adenocarcinoma and lung squamous cell carcinoma were estimated using multiple well-established tumor immune estimation resources, including TIMER, CIBERSORT, and XCell based on the bulk RNA sequencing (RNA-seq) data, as previously described (26–28). The association between estimated immune infiltrates and *ATM* mutation status were evaluated by Wilcoxon rank sum test.

Digital pathology assessment of tumor-infiltrating lymphocytes

Hematoxylin and eosin (H&E) slides were digitalized using Aperio ScanScope AT (0.49 microns/pixel, Leica Biosystems, Germany). Supervised machine learning algorithms (QuPath v.0.2.3) were employed to build an automated tumor-infiltrating lymphocytes scoring model, as previously described by our group (29).

Statistical analysis

Categorical and continuous variables were summarized using descriptive statistics. The Wilcoxon rank sum test and Kruskal–Wallis test were used to test for differences between continuous variables, and Fisher's exact test was used to test for associations between categorical variables. The Kaplan–Meier methodology was used to estimate event–time distributions, and the Greenwood formula was used to estimate the standard errors of the estimates. Log-rank tests were used to test for differences in event–time distributions, and Cox proportional hazards models were fitted to obtain estimates of HRs in univariate and multivariable models. Given the low prevalence of ATM mutations we looked at all lines and adjusted for the line of immunotherapy in multivariable Cox regression analysis. The adjusted HR (aHR) reported reflects this adjustment. Mutation enrichment and co-mutation or mutually exclusive set of genes in each group were detected by pairwise Fisher's exact test, after FDR correction, as previously described (30). Activating mutations in oncogenes,

and loss-of-function mutations in oncosuppressors as per OncoKB (31) were included in the gene mutation enrichment analysis. All *P* values are two-sided and confidence intervals are at the 95% level, with statistical significance defined as $P \leq 0.05$. All statistical analyses were performed using R version 3.6.1

Data availability statement

The data that support the findings of this study are available from the corresponding author upon reasonable request.

Results

Patient characteristics

A total of 5,172 patients with NSCLC whose tumors underwent tumor genomic profiling at DFCI and MSK were identified (DFCI, $N = 3,800$; MSK, $N = 1,372$). The median age of patients in the entire cohort was 66 years (range, 18–99), the majority had non-squamous histology (89.2%), history of tobacco use (81.0%), were female (57.1%), and had stage IV disease at the time of tumor profiling (60.2%). Baseline clinicopathologic features of these patients are reported in Supplementary Table S1.

ATM mutation and baseline clinicopathologic and genomic characteristics

A total of 714 *ATM* mutations were identified in 12.5% (648/5,172) of NSCLC samples which underwent genomic profiling (Supplementary Fig. S1A). Of these, 562 mutations were considered to be deleterious, including loss-of-function mutations and missense mutations predicted to be pathogenic, and occurred in 9.7% (503/5,172) of samples (Fig. 1A), which were considered ATM^{MUT}. 209 (37.2%) mutations were nonsense, ins/del, and splice site mutations (which we designated as class I mutations), while the remaining 353 (62.8%) were predicted pathogenic missense mutations (which we designated as class II mutations; Fig. 1B). Among cases with *ATM* copy-number alteration data available, *ATM* putative LOH was considered present in 14.1% (65/461) of ATM^{MUT} cases, based on concomitant *ATM* copy deletion. Samples without *ATM* mutations or with only *ATM* missense mutations predicted to be benign were considered ATM^{WT}. Benign *ATM* mutations are shown in Supplementary Fig. S1B. Among the 3,800 patients with full genomic data available at the DFCI, we identified 226 potential germline *ATM* variants (including both pathogenic and benign alterations) among 192 (5%) unique patients, based on tumor DNA sequencing data. The full list of potential *ATM* germline variants is shown in Supplementary Table S2.

We next examined differences in clinicopathologic and genomic factors between ATM^{MUT} and ATM^{WT} cases. The baseline clinicopathologic features of patients with ATM^{MUT} and ATM^{WT} NSCLC are shown in Supplementary Table S3. Patients with ATM^{MUT} NSCLC were more likely to be women (62.2% vs. 56.5%; $P = 0.02$), to have non-squamous histology (93.0% vs. 88.7%; $P = 0.004$), and more likely to be ever smokers (89.2% vs. 80.1%; $P < 0.001$). Median TMB, as assessed by the DFCI OncoPanel and MSK-IMPACT NGS platforms was significantly higher among ATM^{MUT} NSCLC compared with ATM^{WT} cases in both cohorts [DFCI: 9.1 vs. 11.0 mutations/megabase (mut/Mb), $P < 0.0001$; MSK:

6.7 vs. 9.7 mut/Mb, $P < 0.0001$; Fig. 1C]. Similarly, median PD-L1 tumor proportion score was also significantly higher among ATM^{WT} (10% vs. 3%; $P = 0.02$; Fig. 1D). ATM^{MUT} cases had a higher proportion of PD-L1 positivity (PD-L1 TPS ≥ 1%) compared with ATM^{WT} cases (72.8% vs. 64.4%, $P = 0.01$). The proportion of samples with PD-L1 expression levels ≥50% (31.5% vs. 28.9%; $P = 0.34$) and ≥ 90% (15.1% vs. 11.6%; $P = 0.08$) was also numerically higher in the ATM^{MUT} group compared with ATM^{WT} (Supplementary Fig. S2).

Among 340 ATM^{MUT} NSCLCs with complete sequencing data available at the DFCI, the most common co-mutated genes included *KRAS* (52%), *TP53* (32%), *STK11* (23%), *KMT2D* (15%), and *KEAP1* (13%; Fig. 2). In comparing ATM^{MUT} versus ATM^{WT} NSCLCs, we identified that *KRAS*, *STK11*, and *ARID2* oncogenic mutations were significantly enriched among ATM^{MUT} NSCLCs ($Q < 0.05$), while *TP53* and *EGFR* mutations were enriched in ATM^{WT} NSCLCs (Fig. 1E). We also interrogated all NSCLCs with *KRAS* allele data available at the DFCI, and confirmed that the most common *KRAS* mutation that occurred in ATM^{MUT} NSCLC included *KRAS* G12C (42.7%), followed by G12V (19.0%), G12A (9.5%, G12F/R/S/I (5.1%), codon 61 mutations (6.2%), and lastly codon 13 mutations (4.3%). When we analyzed co-occurring mutations of other genes among ATM^{MUT} tumors, we found a significant co-occurrence of mutations in *KRAS/STK11*, *STK11/KEAP1*, *SMARCA4/KEAP1*, and *TP53/CDKN2A* in this cohort of NSCLC samples (Supplementary Fig. S3A). These patterns appeared similar to those observed among ATM^{WT} NSCLCs (Supplementary Fig. S3B). However, given the larger sample size of ATM^{WT} NSCLCs, additional co-mutation associations were observed in this cohort. Of note, there were no oncogenic gene mutations enriched among NSCLCs harboring *ATM* missense mutations that were predicted to be benign when compared with NSCLCs without any *ATM* mutation (Supplementary Fig. S4A). To validate our findings in an independent cohort, we analyzed the genomic profiles of ATM^{MUT} and ATM^{WT} NSCLCs in the TCGA dataset. We confirmed that ATM^{MUT} samples were significantly enriched in *KRAS* and *STK11* mutations, while *TP53* alterations were in ATM^{WT} cases ($Q < 0.05$; Supplementary Fig. S4B).

ATM mutation classes correlates with ATM expression by IHC in NSCLC

Among 648 NSCLCs harboring at least one *ATM* mutation, 182 samples (28.1%) from the DFCI cohort underwent ATM IHC. Among these, 143 samples had deleterious mutations [including loss-of-function mutations (class I) and missense mutations predicted to be pathogenic (class II)], while 39 had missense mutations predicted to be benign. 41.8% (76/182) of samples exhibited complete ATM loss by IHC, while the remaining 58.2% (106/182) retained complete ($N = 84/106$) or heterogenous ($N = 22/106$) ATM expression.

We noted that tumors with a class I mutation were significantly more likely to display complete ATM loss by IHC compared with tumors with class II *ATM* mutations only (71.4% vs. 28.6%; $P < 0.0001$; Fig. 3A). Consistently, when we examined the impact of individual *ATM* mutation subtypes and ATM expression by IHC, we identified that ATM expression was retained in 71.4% of samples harboring any missense mutation (including predicted pathogenic and predicted benign mutations), 60.0% of splice site mutations, and

in only 20.7% and 8.3% of tumors with nonsense and ins/del mutations, respectively ($P < 0.0001$; Fig. 3B). Because missense mutations were highly heterogeneous in term of ATM expression by IHC, we next examined whether those mutations resulting in complete ATM loss were closer to splicing sites. Therefore, we calculated the genomic distance in base pairs between each missense mutation and the closest splicing site and found no correlation between ATM expression by IHC and the relative distance of each of these mutations from the nearest splicing site (Supplementary Fig. S5A and B). As a fraction of these samples had concurrent *ATM* mutation and copy loss, suggesting biallelic inactivation, we next asked whether these NSCLCs where LOH was considered present were more likely to lose ATM expression. As expected, we found that cases considered to have LOH had a significantly higher rate of complete ATM loss by IHC, compared with those without LOH (65.2% vs. 38.4%; $P = 0.02$; Supplementary Fig. S5C).

We next determined whether those with complete ATM loss by IHC were associated with different clinicopathologic and genomic characteristics compared with those who retained ATM protein expression. We found that patients whose tumors exhibited complete loss of ATM expression were significantly more likely to be ever smokers (94.7% vs. 81.1%; $P = 0.007$) compared with those whose tumors retained ATM expression (Supplementary Table S4). There was no difference in TMB and PD-L1 distribution between the two groups (Supplementary Fig. S6A and B). We then compared the co-mutation profiles of ATM^{MUT} NSCLCs with or without complete loss of ATM expression by IHC. Importantly, we identified that tumors with complete ATM loss had a higher proportion of *KRAS* mutations (68% vs. 38%; $Q < 0.05$), while those that retained ATM expression by IHC were significantly enriched in *TP53* mutations (47% vs. 17%; $Q < 0.05$), ARID2 (10% vs. 0%; $P < 0.05$), and SETD2 mutations (10% vs. 0%; $P < 0.05$; Fig. 4A and B).

We next focused exclusively on deleterious *ATM* mutations. Among the 143 NSCLCs with deleterious *ATM* mutations, we confirmed that class I mutations (nonsense, insertions/deletions, splice site) were significantly more likely to result in ATM loss by IHC, compared with class II mutations (pathogenic missense mutations; 58.8% vs. 21.3%; $P < 0.0001$; Supplementary Fig. S7A and B). Between missense mutations predicted to be benign and missense mutations predicted to be pathogenic, we did not identify significant differences in the rate of ATM loss by IHC (20.5% vs. 32.2%; $P = 0.20$; Supplementary Fig. S7C).

A full list of the specific *ATM* variants with intact and lost ATM expression by IHC is reported in Supplementary Table S5. Lollipop plots showing *ATM* mutations resulting in complete ATM loss or intact expression by IHC are represented in Fig. 3C and D.

Importantly, among NSCLC samples with any degree of ATM expression we noted that a subset of cases had heterogenous loss (22/106), as highlighted in a representative case in Fig. 3E and F. Therefore, we lastly sought to dissect the characteristics of these tumors. We noted that patients with ATM heterogenous loss had more similar clinicopathologic and genomic features compared with those with completely intact ATM expression. Similar to cases with intact ATM expression, patients with heterogenous loss were more likely be never smokers compared with those with complete ATM loss, and had lower frequency of concurrent *KRAS* and *STK11* mutations and higher rates of *TP53* mutations compared with

NSCLC with complete ATM loss by IHC (Supplementary Table S6; Supplementary Fig. S8).

Impact of *ATM* mutation and ATM loss by IHC on clinical outcomes in NSCLC

We next aimed to determine whether *ATM* mutation status was associated with clinical outcomes in patients with NSCLC. There was no difference in disease-free survival (DFS) and overall survival (OS) among patients with stage I andstage IINSCLC (Supplementary Fig. S9A and B). Similarly, among all comers with stage III NSCLC there was no impact of *ATM* mutation status on DFS and OS (Supplementary Fig. S10A and B). When we restricted our analysis to patients with unresectable stage III NSCLC who received concurrent chemo-radiotherapy followed by durvalumab maintenance we did not observe differences in DFS and OS according to *ATM* mutation status (Supplementary Fig. S10C and D). When we analyzed the impact of *ATM* mutations on OS in all comers with stage IV NSCLC, we again did not find differences between ATM^{MUT} and ATM^{WT} NSCLCs (Supplementary Fig. S11). We also examined whether among ATM^{MUT} tumors those with complete ATM loss had different clinical outcomes compared with those that retained ATM expression. Similarly, we did not observe differences in DFS and OS instage I, stage II, and stage III NSCLC, and in OS in all comers with stage IV NSCLC according to ATM expression by IHC (Supplementary Fig. S12A–C; Supplementary Fig. S13).

In a subset of patients treated with PD-(L)1 immune checkpoint blockade monotherapy ($N = 1{,}522$), primarily in the second- or subsequent-line setting (63.8%, because this is a historical cohort), we found no difference between ATM^{MUT} and ATM^{WT} cases in terms of ORR (25.2% vs. 22.7%; $P = 0.55$), PFS (2.7 vs. 3.2 months; aHR, 1.03; $P = 0.77$) and OS (14.3 vs. 13.6 months; aHR, 1.06; $P = 0.60$; Fig. 5A–C).

In a subset of patients treated with PD-(L)1 immune checkpoint blockade in combination with platinum doublet chemotherapy ($N = 951$), primarily in the first-line setting (88.6%), we did not observe statistically significant differences in ORR, PFS, and OS by *ATM* mutation status. The ORR was numerically greater in the ATM^{MUT} group versus the ATM^{WT} group (45.1% vs. 36.9%; $P = 0.15$; Fig. 5D–F).

When we examined clinical outcomes to both PD-(L)1 immune checkpoint blockade monotherapy and PD-(L)1 immune checkpoint blockade in combination with platinum doublet chemotherapy within each clinically relevant PD-L1 expression subset of < 1%, 1% to 49%, and ≥ 50%, we did not observe statistically significant differences in ORR, PFS, and OS by *ATM* mutation status (Supplementary Fig. S14; Supplementary Fig. S15). For patients who received PD-(L)1 immune checkpoint blockade, ORR was numerically greater in the ATM^{MUT} group versus the ATM^{WT} group within the 1% to 49% (50.0% vs. 36.9%; $P = 0.21$) and ≥ 50% (64.3% vs. 50.5%; $P = 0.49$) PD-L1 expression subsets, but not the < 1% PD-L1 expression subset (32.1% vs. 33.4%; $P = 1.0$).

As concurrent *ATM*/*TP53* mutations have been previously reported to correlate with improved immunotherapy efficacy in NSCLC (32), we also explored whether in our cohort there was a similar effect. Among patients treated with PD-(L)1 immune checkpoint blockade monotherapy, we noted that ORR was highest among patients with concurrent

ATM/TP53 mutation (35.7%), as compared with patients with $ATM^{MUT}/TP53^{WT}$ (20.0%), $ATM^{WT}/TP53^{MUT}$ (24.2%), $ATM^{WT}/TP53^{WT}$ (20.3%; $P = 0.037$; Supplementary Fig. S16A). Median PFS was also significantly longer among patients with $ATM^{MUT}/TP53^{MUT}$ NSCLCs, compared with patients with ATM^{MUT}, $TP53^{MUT}$, and $ATM^{WT}/TP53^{WT}$ genotype ($P = 0.02$; Supplementary Fig. S16B). There was no statistically significant difference in OS across these 4 groups (Supplementary Fig. S16C). Similarly, we observed numerically greater ORR in the $ATM^{MUT}/TP53^{MUT}$ group [ORR 55.6% vs. 40.0% ($ATM^{MUT}/TP53^{WT}$), 40.1% ($ATM^{WT}/TP53^{MUT}$), and 34.3% ($ATM^{WT}/TP53^{WT}$); $P = 0.06$] among patients who received PD-(L)1 immune checkpoint blockade plus doublet chemotherapy, with no statistically significant difference in PFS and OS (Supplementary Fig. S16D–F). In the subset of patients with any *ATM* mutation which underwent ATM IHC and received treatment with PD-(L)1 immune checkpoint blockade monotherapy, we did not observe differences in ORR (7.7% vs. 14.8%; $P = 1.0$), PFS (2.0 vs. 2.9 months; HR, 0.83; $P = 0.61$), and OS (4.9 vs. 8.4 months; HR, 0.86; $P = 0.68$), according to ATM expression (Supplementary Fig. S17A–C). The same analysis was not deemed to be feasible for patients treated with PD-(L)1 immune checkpoint blockade plus doublet chemotherapy due to limited sample size.

Our group has recently reported that *STK11* and *KEAP1* mutations are associated with primary resistance to PD-(L)1 monotherapy (33) and chemoimmunotherapy (34) in patients with advanced NSCLC. Because we noted a significant enrichment in *STK11* mutations among ATM^{MUT}cancers in this study, we next interrogated whether concurrent *STK11* or *KEAP1* mutation was associated with clinical outcomes to PD-(L)1 immune checkpoint blockade in patients with ATM^{MUT}. Importantly we noted no statistically significant difference in ORR, PFS, and OS to PD-(L)1 immune checkpoint blockade with or without platinum doublet chemotherapy between *STK11* mutant and *STK11* wild-type NSCLCs, among ATM^{MUT} patients (Supplementary Fig. S18A–F). Similarly, among ATM^{MUT} NSCLCs, we did not observe statistically significant differences in ORR, PFS, and OS to PD-(L1) immune checkpoint blockade between *KEAP1*-mutant and *KEAP1*–wild-type cases (Supplementary Fig. S19A–F). Together, these data suggest that *STK11* and *KEAP1* co-mutations may not necessarily impact clinical outcomes to PD-(L)1 immune checkpoint blockade among ATM^{MUT} NSCLC, possibly because of the higher TMB and PD-L1 expression that characterize ATM^{MUT} NSCLC, compared with ATM^{WT} cases.

Impact of *ATM* mutation on tumor infiltrating immune cells in NSCLC

To determine whether *ATM* mutations also impacted tumor associated immune cells, we next examined the immunophenotype in a subset of NSCLC samples ($n = 535$) which underwent mIF at the DFCI. The baseline clinicopathologic features of patients whose tumors underwent mIF are summarized in Supplementary Table S7. We found no difference in intratumoral, TSI and total $CD8^+$, $PD1^+$, $CD8^+PD1^+$, and $Foxp3^+$ T cells between ATM^{MUT} and ATM^{WT} NSCLCs (Supplementary Fig. S20; Supplementary Fig. S21). Similarly, we did not observe differences in the proportion of tumor, non-tumor, and total $PD\text{-}L1^+$ cells between ATM^{MUT} *and* ATM^{WT} tumors (Supplementary Fig. S22). Among ATM^{MUT} NSCLC, there was significant positive correlation between intratumoral and TSI $CD8^+$, $PD1^+$, $CD8^+PD1^+$, and $Foxp3^+$ T cells, as well as between tumoral and non-tumoral

PD-L1^{+} cells (Supplementary Fig. S23), indicating similar density of tumor associated immune cells at the stroma interface and intratumorally.

Interestingly, when we examined the impact of *ATM/TP53* co-mutation status on NSCLC immunophenotype, we noted that *ATM*^{MUT}/*TP53*^{MUT} tumors had the highest proportion of TSI CD8^{+} ($P < 0.001$) T cells, as well as tumor ($P = 0.001$), non-tumor ($P = 0.003$), and total ($P = 0.002$) PD-L1^{+} cells (Supplementary Fig. S24; Supplementary Fig. S25; Supplementary Fig. S26), when compared with the *ATM*^{MUT}/*TP53*^{WT}, *ATM*^{WT}/*TP53*^{MUT}, *and ATM*^{WT}/*TP53*^{WT} groups. This finding may reflect the higher TMB levels of *ATM/TP53* co-mutated tumors observed in this cohort (Supplementary Fig. S27), which has been associated with increased immune cell subset infiltration and higher PD-L1 expression levels (35). To further corroborate these findings, we also used computational pathology analysis to quantify tumor-infiltrating lymphocytes on H&E slides, as previously described by our group (29). Again, we did not observe differences in TILs count between *ATM*^{MUT} and *ATM*^{WT} NSCLC (Supplementary Fig. S28A). When we interrogated the impact of *ATM/TP53* co-mutations on TILs distribution, we identified that tumors with *ATM/TP53* co-mutations had the numerically highest TILs count, compared with *ATM*^{MUT}/*TP53*^{WT}, *ATM*^{WT}/*TP53*^{MUT}, and *ATM*^{WT}/*TP53*^{WT} NSCLCs, though this difference was not statistically significant, likely due to the small sample size of these subsets (Supplementary Fig. S28B). To expand our analysis on the immunophenotypic correlates of ATM mutations in NSCLC, we lastly deconvoluted bulk RNA-seq data from the NSCLC-TCGA into immune cell subsets and analyzed the enrichment in immune cells according to *ATM* mutation status. We noted that *ATM*^{MUT} NSCLCs had lower enrichment scores in myeloid dendritic cells, neutrophils and CD4+ effector memory cells ($P < 0.05$; Supplementary Fig. S29), compared with *ATM*^{WT} cases. By contrast, *ATM*^{MUT} NSCLCs had significantly higher enrichment scores in CD4^{+} Th1 cells.

Discussion

We identified that *ATM*^{MUT} tumors harbor distinct clinicopathologic, genomic, and immunophenotypic features including being significantly associated with female sex, ever smoking status, non-squamous histology, PD-L1 expression, higher TMB, and enrichment for co-occurring *KRAS* and *STK11* mutations compared with *ATM*^{WT} tumors (which, in contrast, were enriched for *TP53* and *EGFR* mutations).

To explore the functional consequences of specific *ATM* variants, we integrated genomic data (including *in silico* prediction of missense mutation pathogenicity) with matched ATM IHC data. We identified that loss-of-function mutations were significantly more likely to be associated with complete ATM loss than missense mutations (though of note, the proportion of complete ATM loss for splice site mutations was similar to that of missense mutations). Tumors with putative LOH were also significantly associated with complete ATM loss. However, the substantial heterogeneity of ATM IHC status among missense mutations highlights the real-world challenges in assessing pathogenicity based on knowledge of the variant alone (for example, based on reports from NGS assays available in standard care today), as well as the likely limitations of current *in silico* prediction tools. Supplementary Table S5, which lists the ATM IHC status for 182 tumors harboring 198 *ATM* mutations

in our study may serve as an initial resource to guide interpretation of *ATM* variants in NSCLC, and potentially help prioritize patients for ATR inhibitor or other DDR targeted therapy trials. However, substantially broader functional characterization of *ATM* variants in preclinical models and in correlative works using clinical samples is needed. Further investigation of heterogenous ATM IHC loss is also needed (13). Optimal assessment of *ATM* variants in the clinic may require integration of multiple datapoints [including co-mutations (e.g., *KRAS*, *STK11*, *TP53*, etc.), LOH, ATM IHC, other DDR biomarkers, etc.] to identify those patients that may benefit from DDR-based targeted therapy strategies, or even individualization of standard systemic therapy approaches, as discussed below. In addition, given that *KRAS* mutations are enriched among ATM^{MUT} tumors, an intriguing question is whether co-occurring *ATM* mutations may impact KRAS-directed targeted therapy strategies.

While *ATM* mutation status overall was not associated with statistically significant differences in outcomes to PD-(L)1 immune checkpoint blockade, it should be noted that ATM^{MUT} tumors were significantly enriched in *STK11* mutations, which are important mediators of primary resistance to ICI in NSCLC, particularly in the setting of concurrent *KRAS* mutation (also enriched in ATM^{MUT} tumors). Therefore, our results should be interpreted in the context of the complex and heterogenous genomic profile of ATM^{MUT} NSCLC.

Importantly, in this study we also confirmed that patients with $ATM^{MUT}/TP53^{MUT}$ NSCLC had improved clinical outcomes with PD-(L)1 based therapies, which may be attributable to a higher TMB in patients harboring both deleterious *ATM* and *TP53* mutations. Furthermore, TSI $CD8^{+}$, cells were higher in $ATM^{MUT}/TP53^{MUT}$ tumors, as were tumor, immune, and total PD-$L1^{+}$ cells, which can also contribute to the enhanced sensitivity to ICI among patients with concurrent *ATM/TP53* mutations. Finally, given that DNA damage and repair genes play a role in radiation repair, loss-of-function mutations in these genes, including *ATM*, can potentially lead to radiation sensitivity and improved locoregional outcomes (36). In our study however, we did not observe differences in clinical outcomes to concurrent chemoradiotherapy followed by durvalumab consolidation, which currently represent the new standard of care for patients with unresectable stage III NSCLC (37).

Our clinical outcomes analyses may be impacted by relatively small sample sizes in the respective treatment groups, and further studies are needed to explore our findings further in larger datasets, including those that include a larger number of patients treated with PD-(L)1 immune checkpoint blockade monotherapy in the first-line setting. Given the limitations of PD-L1 and TMB, as well as the increase in first-line systemic therapy options in advanced/metastatic NSCLC, including those only involving PD-(L)1 immune checkpoint blockade alone (or along with CTLA-4 inhibition) without platinum doublet chemotherapy, additional biomarkers are needed to optimally guide clinical decision-making. In the future, this may also be important in the neoadjuvant and adjuvant settings as well (38–40).

The limitations of this study include its retrospective design, population reflecting only two academic cancer centers both located in the Northeastern United States, relatively small sample sizes for ATM IHC as well as treatment outcome analyses, and lack of other

DDR biomarker data. In addition, the pathogenicity of missense mutations of unknown significance was determined using *in silico* tools. Nonetheless, to our knowledge, our study represents the most comprehensive analysis of *ATM* mutations in NSCLC to date, and creates key insights towards advancing potential future precision oncology strategies in ATM^{MUT} NSCLC.

Supplementary Material

Refer to Web version on PubMed Central for supplementary material.

Acknowledgments

This work was supported by the Barbara Wilson Gomez Endowed Fellowship in Thoracic Oncology (to B. Ricciuti), the Conquer Cancer Foundation of ASCO Young Investigator Award (to B. Ricciuti), the International Lung Cancer Foundation Fellowship Award (to B. Ricciuti), and the Elva J. and Clayton L. McLaughlin Fund for Lung Cancer Research (to M.M. Awad). M.L. Cheng acknowledges funding from Conquer Cancer Foundation-American Society of Clinical Oncology Career Development Award and Prostate Cancer Foundation Young Investigator Award.

References

1. Pilié PG, Tang C, Mills GB, Yap TA. State-of-the-art strategies for targeting the DNA damage response in cancer. Nat Rev Clin Oncol 2019;16:81–104. [PubMed: 30356138]
2. Ciccia A, Elledge SJ. The DNA damage response: making it safe to play with knives. Mol Cell 2010;40:179. [PubMed: 20965415]
3. Hanahan D, Weinberg RA. Hallmarks of cancer: the next generation. Cell 2011; 144:646–74. [PubMed: 21376230]
4. Boohaker RJ, Xu B. The versatile functions of ATM kinase. Biomed J 2014; 37:3. [PubMed: 24667671]
5. Choi M, Kipps T, Kurzrock R. ATM mutations in cancer: therapeutic implications. Mol Cancer Ther 2016;15:1781–91. [PubMed: 27413114]
6. Chang MT, Asthana S, Gao SP, Lee BH, Chapman JS, Kandoth C, et al. Identifying recurrent mutations in cancer reveals widespread lineage diversity and mutational specificity. Nat Biotechnol 2016;34:155–63. [PubMed: 26619011]
7. Cerami E, Gao J, Dogrusoz U, Gross BE, Sumer SO, Aksoy BA, et al. The cBio cancer genomics portal: an open platform for exploring multidimensional cancer genomics data. Cancer Discov 2012;2:401–4. [PubMed: 22588877]
8. Jette NR, Kumar M, Radhamani S, Arthur G, Goutam S, Yip S, et al. ATM-deficient cancers provide new opportunities for precision oncology. Cancers 2020;12:687. [PubMed: 32183301]
9. Ding L, Getz G, Wheeler DA, Mardis ER, McLellan MD, Cibulskis K, et al. Somatic mutations affect key pathways in lung adenocarcinoma. Nature 2008; 455:1069–75. [PubMed: 18948947]
10. Villaruz LC, Jones H, Dacic S, Abberbock S, Kurland BF, Stabile LP, et al. ATM protein is deficient in over 40% of lung adenocarcinomas. Oncotarget 2016;7: 57714–25. [PubMed: 27259260]
11. Petersen LF, Klimowicz AC, Otsuka S, Elegbede AA, Petrillo SK, Williamson T, et al. Loss of tumor-specific ATM protein expression is an independent prognostic factor in early resected NSCLC. Oncotarget 2017;8:38326–36. [PubMed: 28418844]
12. Weber AM, Drobnitzky N, Devery AM, Bokobza SM, Adams RA, Maughan TS, et al. Phenotypic consequences of somatic mutations in the ataxia-telangiectasia mutated gene in non--small cell lung cancer. Oncotarget 2016;7:60807–22. [PubMed: 27602502]
13. Ditano JP, Donahue KL, Tafe LJ, McCleery CF, Eastman A. Sensitivity of cells to ATR and CHK1 inhibitors requires hyperactivation of CDK2 rather than endogenous replication stress or ATM dysfunction. Sci Rep 2021;11:7077. [PubMed: 33782497]

14. Reaper PM, Griffiths MR, Long JM, Charrier J-D, MacCormick S, Charlton PA, et al. Selective killing of ATM- or p53-deficient cancer cells through inhibition of ATR. Nat Chem Biol 2011;7:428–30. [PubMed: 21490603]
15. Rafiei S, Fitzpatrick K, Liu D, Cai M-Y, Elmarakeby HA, Park J, et al. ATM loss confers greater sensitivity to ATR inhibition than PARP inhibition in prostate cancer. Cancer Res 2020;80:2094–100. [PubMed: 32127357]
16. Hall AB, Newsome D, Wang Y, Boucher DM, Eustace B, Gu Y, et al. Potentiation of tumor responses to DNA damaging therapy by the selective ATR inhibitor VX-970. Oncotarget 2014;5:5674–85. [PubMed: 25010037]
17. Yap TA, O'Carrigan B, Penney MS, Lim JS, Brown JS, de Miguel Luken MJ, et al. Phase I trial of first-in-class ATR inhibitor M6620 (VX-970) as monotherapy or in combination with carboplatin in patients with advanced solid tumors. J Clin Oncol 2020;38:3195–204. [PubMed: 32568634]
18. Yap TA, Tan DSP, Terbuch A, Caldwell R, Guo C, Goh BC, et al. First-in-human trial of the oral ataxia telangiectasia and RAD3-related (ATR) inhibitor BAY 1895344 in patients with advanced solid tumors. Cancer Discov 2021;11:80–91. [PubMed: 32988960]
19. Plummer R, Dean E, Arkenau H-T, Redfern C, Spira AI, Melear JM, et al. A phase Ib study evaluating the safety and preliminary efficacy of berzosertib in combination with gemcitabine in patients with advanced non--small cell lung cancer. Lung Cancer 2022;163:19–26. [PubMed: 34894455]
20. Middleton MR, Dean E, Evans TRJ, Shapiro GI, Pollard J, Hendriks BS, et al. Phase I study of the ATR inhibitor berzosertib (formerly M6620, VX-970) combined with gemcitabine cisplatin in patients with advanced solid tumors. Br J Cancer 2021;125:510–9. [PubMed: 34040175]
21. Ricciuti B, Recondo G, Spurr LF, Li YY, Lamberti G, Venkatraman D, et al. Impact of DNA damage response and repair (DDR) gene mutations on efficacy of PD-(L)1 immune checkpoint inhibition in non–small cell lung cancer. Clin Cancer Res 2020;26:4135–42. [PubMed: 32332016]
22. Xiong A, Nie W, Zhou Y, Li C, Gu K, Zhang D, et al. Comutations in DDR pathways predict atezolizumab response in non--small cell lung cancer patients. Front Immunol 2021;12:708558. [PubMed: 34630387]
23. Garcia EP, Minkovsky A, Jia Y, Ducar MD, Shivdasani P, Gong X, et al. Validation of OncoPanel: a targeted next-generation sequencing assay for the detection of somatic variants in cancer. Arch Pathol Lab Med 2017;141:751–8. [PubMed: 28557599]
24. Sholl LM, Do K, Shivdasani P, Cerami E, Dubuc AM, Kuo FC, et al. Institutional implementation of clinical tumor profiling on an unselected cancer population. JCI Insight 2016;1:e87062. [PubMed: 27882345]
25. Cheng DT, Mitchell TN, Zehir A, Shah RH, Benayed R, Syed A, et al. Memorial Sloan Kettering—integrated mutation profiling of actionable cancer targets (MSK-IMPACT): a hybridization capture-based next-generation sequencing clinical assay for solid tumor molecular oncology. J Mol Diagn 2015;17:251–64. [PubMed: 25801821]
26. Newman AM, Liu CL, Green MR, Gentles AJ, Feng W, Xu Y, et al. Robust enumeration of cell subsets from tissue expression profiles. Nat Methods 2015; 12:453–7. [PubMed: 25822800]
27. Aran D, Hu Z, Butte AJ. xCell: digitally portraying the tissue cellular heterogeneity landscape. Genome Biol 2017;18:220. [PubMed: 29141660]
28. Li T, Fan J, Wang B, Traugh N, Chen Q, Liu JS, et al. TIMER: a web server for comprehensive analysis of tumor-infiltrating immune cells. Cancer Res 2017;77: e108–10. [PubMed: 29092952]
29. Rakaee M, Adib E, Ricciuti B, Sholl LM, Shi W, Alessi JV, et al. Association of machine learning–based assessment of tumor-infiltrating lymphocytes on standard histologic images with outcomes of immunotherapy in patients with NSCLC. JAMA Oncol 2023;9:51. [PubMed: 36394839]
30. Mayakonda A, Lin D-C, Assenov Y, Plass C, Koeffler HP. Maftools: efficient and comprehensive analysis of somatic variants in cancer. Genome Res 2018;28: 1747–56. [PubMed: 30341162]
31. Chakravarty D, Gao J, Phillips SM, Kundra R, Zhang H, Wang J, et al. OncoKB: a precision oncology knowledge base. JCO Precis Oncol 2017;2017: PO.17.00011.
32. Chen Y, Chen G, Li J, Huang Y-Y, Li Y, Lin J, et al. Association of tumor protein p53 and ataxia-telangiectasia mutated comutation with response to immune checkpoint inhibitors and mortality

in patients with non--small cell lung cancer. JAMA Netw open 2019;2:e1911895. [PubMed: 31539077]

33. Ricciuti B, Arbour KC, Lin JJ, Vajdi A, Vokes N, Hong L, et al. Diminished efficacy of programmed death-(ligand)1 inhibition in STK11- and KEAP1-mutant lung adenocarcinoma is affected by KRAS mutation status. J Thorac Oncol 2022;17:399–410. [PubMed: 34740862]
34. Alessi JV, Elkrief A, Ricciuti B, et al. Clinicopathologic and genomic factors impacting efficacy of first-line chemoimmunotherapy in advanced non--small cell lung cancer (NSCLC). J Thorac Oncol 2023;S1556–0864:00121–1.
35. Ricciuti B, Wang X, Alessi JV, Rizvi H, Mahadevan NR, Li YY, et al. Association of high tumor mutation burden in non–small cell lung cancers with increased immune infiltration and improved clinical outcomes of PD-L1 blockade across PD-L1 expression levels. JAMA Oncol 2022;8:1160–8. [PubMed: 35708671]
36. Pitter KL, Casey DL, Lu YC, Hannum M, Zhang Z, Song X, et al. Pathogenic ATM mutations in cancer and a genetic basis for radiotherapeutic efficacy. J Natl Cancer Inst 2021;113:266–73. [PubMed: 32726432]
37. Antonia SJ, Villegas A, Daniel D, Vicente D, Murakami S, Hui R, et al. Durvalumab after chemoradiotherapy in stage III non–small cell lung cancer. N Engl J Med 2017;377:1919–29. [PubMed: 28885881]
38. Provencio M, Calvo V, Romero A, Spicer JD, Cruz-Bermúdez A. Treatment sequencing in resectable lung cancer: the good and the bad of adjuvant versus neoadjuvant therapy. Am Soc Clin Oncol Educ B 2022;42:711–28.
39. Felip E, Altorki N, Zhou C, Csőszi T, Vynnychenko I, Goloborodko O, et al. Adjuvant atezolizumab after adjuvant chemotherapy in resected stage IB–IIIA non–small cell lung cancer (IMpower010): a randomized, multicenter, open-label, phase III trial. Lancet 2021;398:1344–57. [PubMed: 34555333]
40. Forde PM, Spicer J, Lu S, Provencio M, Mitsudomi T, Awad MM, et al. Neoadjuvant nivolumab plus chemotherapy in resectable lung cancer. N Engl J Med 2022;386:1973–85. [PubMed: 35403841]

Translational Relevance

In this study, we identified that *ATM*-mutant tumors harbor distinct clinicopathologic, genomic, and immunophenotypic features including being significantly associated with female sex, ever smoking status, non-squamous histology, programmed death-ligand 1 expression, higher tumor mutational burden, and enrichment for co-occurring *KRAS* and *STK11* mutations compared with *ATM*–wild-type tumors. To explore the functional consequences of specific *ATM* variants, we integrated genomic data with matched ATM IHC data and found that loss-of-function mutations are significantly more likely to be associated with complete ATM loss than missense mutations highlighting the real-world challenges in assessing pathogenicity based on knowledge of the variant alone. These results can guide interpretation of *ATM* variants in non–small cell lung cancer, and potentially help prioritize patients for ataxia telangiectasia and Rad3-related inhibitor or other DNA damage and repair targeted therapy trials, as well as precision immune checkpoint blockade treatment approaches.

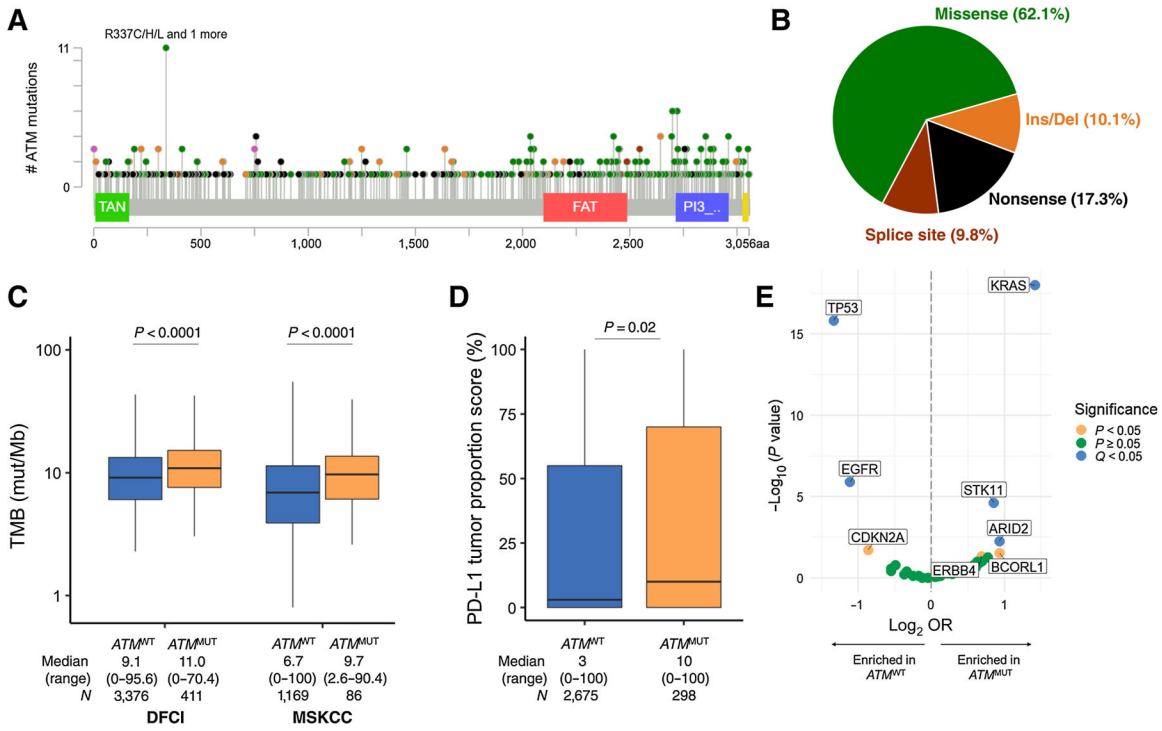

Figure 1.

A, Lollipop plot showing 485 deleterious *ATM* mutations identified in the DFCI/MSK cohort. **B,** Pie chart showing the frequency of deleterious missense, nonsense, insertions/deletions, and splice site mutation in the combined DFCI/MSK cohort (**C**) TMB distributions in ATM^{WT} and ATM^{MUT} NSCLCs in the DFCI and MSK cohorts. **D,** Distribution of PD-L1 tumor proportion score in ATM^{WT} and ATM^{MUT} NSCLCs. **E,** Volcano plot showing oncogenic gene mutations enriched in ATM^{WT} and ATM^{MUT} NSCLCs.

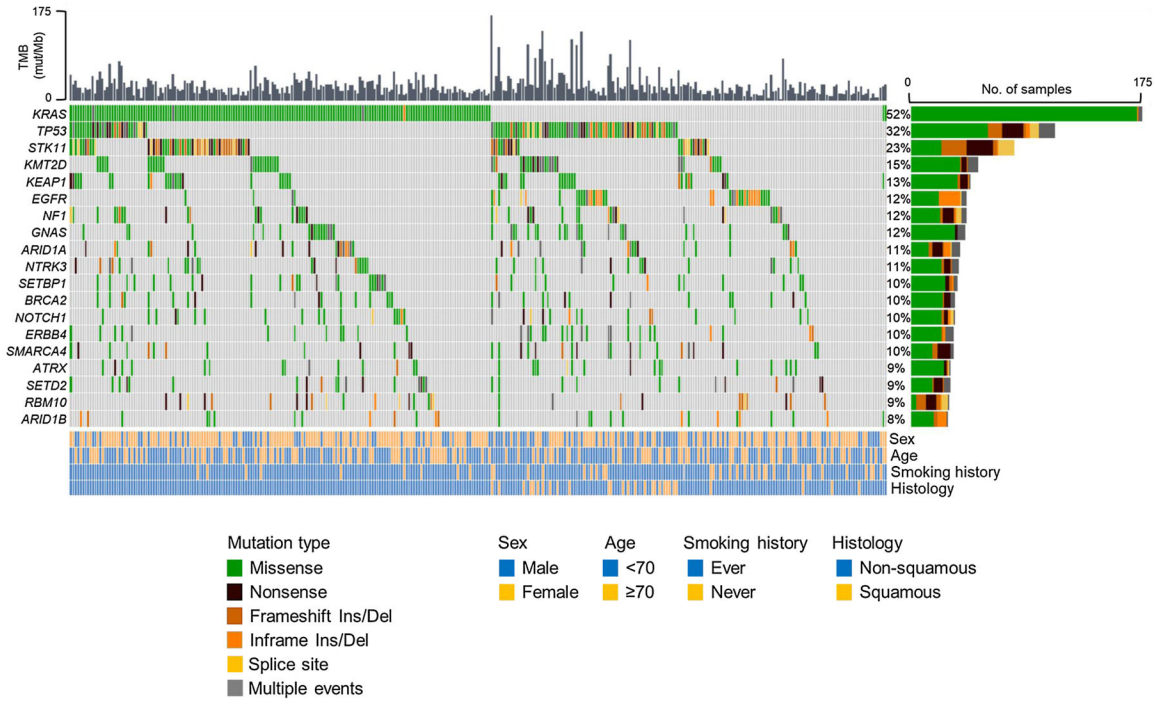

Figure 2.

Oncoprint plot showing the genomic profiles of *ATM*^{MUT} NSCLCs in the DFCI genomic cohort. The most frequent 20 genes that are mutated are shown.

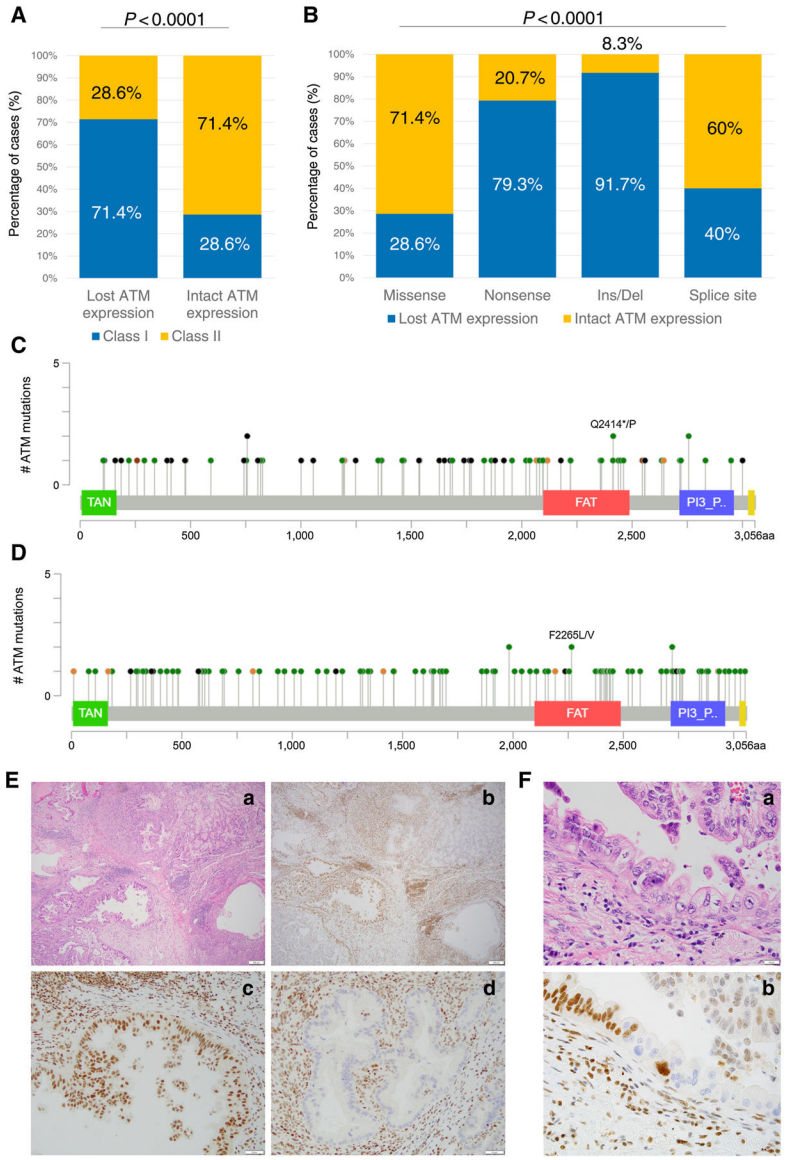

Figure 3.

A, Histograms showing the distribution of class I and class II *ATM* mutations with lost or intact ATM protein expression by IHC. **B,** Histograms showing the distribution of missense, nonsense, splice site, and ins/del mutations with lost or intact ATM protein expression by IHC. **C,** Lollipop plot of *ATM* mutations resulting in complete ATM loss by IHC. **D,** Lollipop plot of *ATM* mutations with intact (including heterogeneous loss) ATM expression by IHC. **E,** H&E low power view of a lung adenocarcinoma (**a**) that shows heterogeneous expression or ATM (**b**) including strong expression in a micropapillary component (**c**) and complete absence in the acinar component with mucinous differentiation (**d**). **F,** H&E high power view of a lung adenocarcinoma (**a**) with multiple intermingled subclones visualized with differing levels of ATM including strong (top left), intermediate/weak (top right), and complete loss (bottom right) (**b**). Background stromal and inflammatory cells show strong nuclear expression of ATM, as expected.

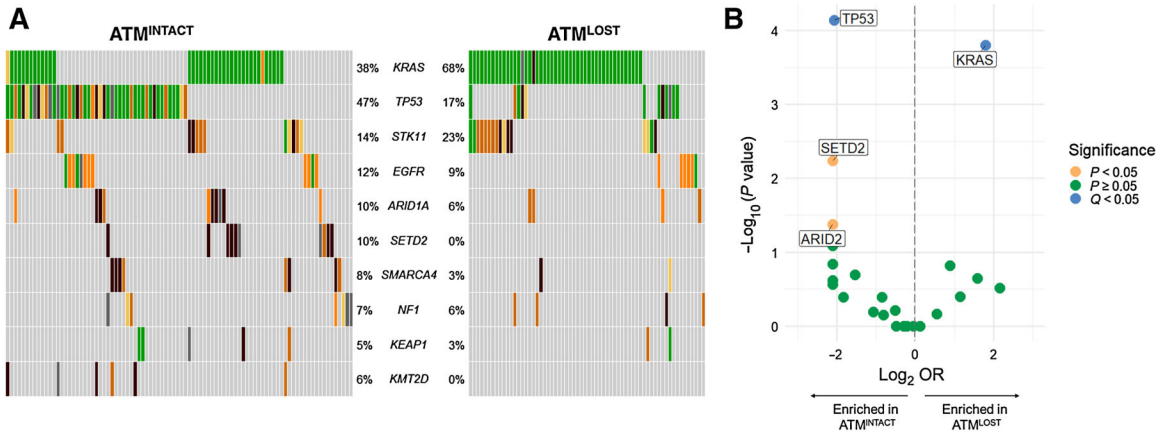

Figure 4.

A, Oncoprint plot showing the most commonly mutated genes in *ATM* mutated NSCLCs according to ATM expression by IHC (lost vs. intact). **B,** Volcano plot showing gene mutations significantly enriched in *ATM*^{MUT} NSCLCs with versus without complete ATM loss by IHC.

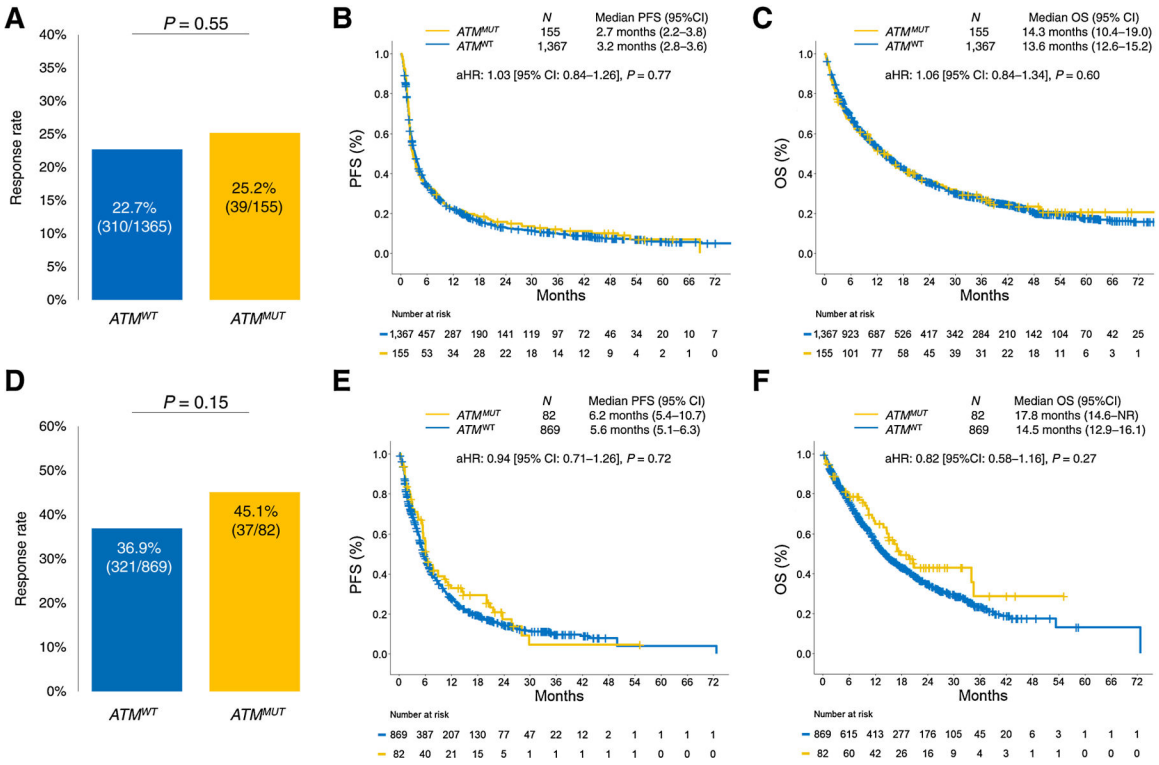

Figure 5.

A, ORR, (**B**) PFS, and (**C**) OS to PD-(L)1 immune checkpoint blockade monotherapy, primarily in the second- or subsequent line setting, among patients with advanced NSCLC, according to *ATM* mutation status. **D,** ORR, (**E**) PFS, and (**F**) OS to PD-(L)1 immune checkpoint blockade plus platinum doublet chemotherapy, primarily in the first-line setting, among patients with advanced/metastatic NSCLC, according to *ATM* mutation status.